Model for the propagation of sound in granular materials

Michael Leibig*
Höchstleistungsrechenzentrum, Kernforschungsanlage Jülich, Postfach 1913, 5170 Jülich, Germany
(Received 1 February 1993; revised manuscript received 18 October 1993)

This paper presents a simple model for the propagation of small-amplitude vibrations in a granular material. In this model, the grains are taken to be spherical balls that interact via linear springs. The positional disorder in the real system is ignored and the particles are placed on the vertices of a square lattice. The only disorder in the system comes from a random distribution of the spring constants. Despite its apparent simplicity, this model is able to reproduce the complex frequency response seen in measurements of sound propagation in a granular system. In order to understand this behavior, the role of the resonance modes of the system is investigated. Finally, this simple model is generalized to include relaxation behavior in the force network—a behavior which is also seen in real granular materials. This model gives quantitative agreement with experimental observations of relaxation.

PACS number(s): 43.40.+s, 63.50.+x, 05.40.+j, 46.10.+z

I. INTRODUCTION

Understanding the properties of granular materials presents a difficult challenge to condensed-matter science [1]. A fundamental property of any material is its response to small-amplitude vibrations. For the case of solids, the behavior of the system is characterized by the phonon spectrum. These elementary excitations for perfect crystals are well understood, but for disordered systems, the situation is not so clear. When disorder is present, localization of these excitation can occur [2], and while much progress has been made in understanding the phenomena of localization, there are still many fundamental properties that remain a mystery [3].

While there have been many studies of the localized modes in disordered systems [4–6], there has been less attention paid to the response of these systems to a periodic driving force [7]. Generally speaking, for a uniform periodically driven linear system in the long-time limit, the frequency of oscillation is that of the forcing [8]. As the frequency of the driver goes through a resonant frequency, the amplitude of the motion is increased, and the oscillations take on the character of the corresponding normal mode. Does this picture reman for the case of a disordered granular material which has complicated nonlinear interparticle interactions? In these systems, there is known to be a network of contact forces with a complex structure. The phenomena of arching suggest that this system is supported by a small fraction of grains which have a high concentration of stress, while most of the particles remain in loose contact [9]. The response of this system to driving may then depend wholly on the structure of this network where the stress is highly concentrated.

In this paper, I discuss a model system of balls and springs that can reproduce many of the vibrational properties of a real granular system. The numerical results that come from this model will be compared with the results from a beautiful set of experiments performed by Liu and Nagel in which they measured the response of a single "grain of sand" to an external driving force [10]. I describe briefly these experiments and summarize the important results. The experimental apparatus consisted of a rigid box filled with glass beads of diameter $d=0.5$ cm. The box itself was 28×28 cm^2 and was filled with beads up to heights of 8–15 cm. The upper layer of the bead pack was a free surface. An aluminum disk that was attached to an external speaker was placed at one end of the box. The speaker could be driven with varying frequencies and amplitudes. Inside the bead pack was an accelerometer which was roughly the size of one bead. This device was sensitive only to horizontal accelerations, and was unaffected by sound waves propagating through the surrounding air. Since this detector was comparable to the size of a bead, it is effectively measuring the motion of a single particle under the action of the driving vibration. The motion of the aluminum disk was also monitored with an accelerometer attached directly to it.

The disk was driven with an acceleration of the form $A_s\sin(\omega t)$ and the detector was found to oscillate as $A_d(t)\sin[\omega t+\phi(t)]$, where $A_d(t)$ and $\phi(t)$ were the detector amplitude and phase shift, respectively. Both of these functions were found to vary slowly with time. Figure 1(a) shows $A_d(t)$ with a driving frequency $\omega=637$ sec^{-1}, and $A_s=1.4g$ where g is the acceleration of gravity. Note that the time scale for the changes in $A_d(t)$ is much longer than the time scale for the oscillation itself. The power spectrum [shown in Fig. 1(b)] of this time series shows a power-law region with exponent ≈-2 at frequencies from 10^{-5} to 10^{-1} Hz.

On time scales of the order of a few oscillations, however, the amplitude at a given driving frequency is fixed. This inspired a second set of measurements using the same experimental setup. With a fixed acceleration for the driving force, the amplitude of the detector is measured for various values of ω. Let the response function $\eta(\omega)=A_d/A_s$ for a driving frequency ω. This ratio is plotted as a function of ω in Fig. 2. The two curves

*Present address: ITP, University of California, Santa Barbara, CA 93106.

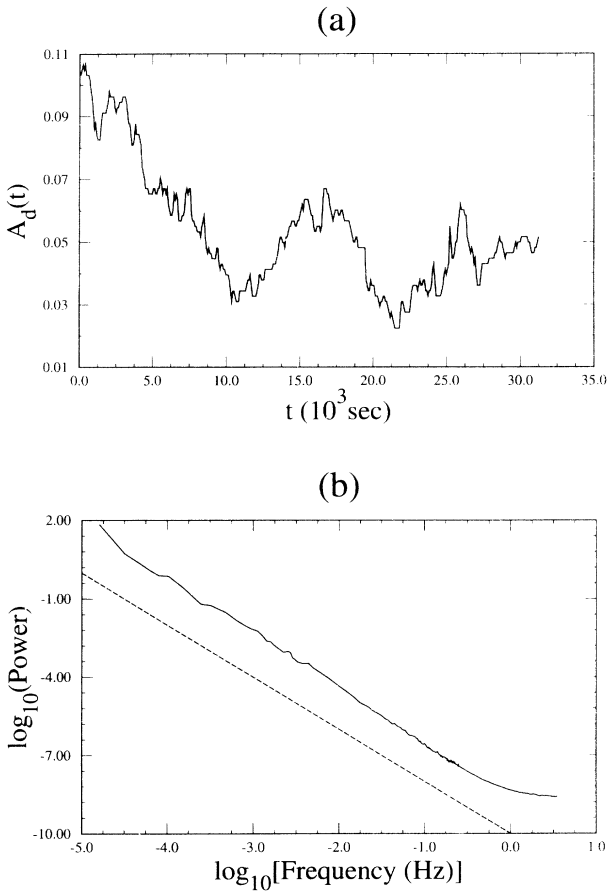

FIG. 1. Experimental results for the amplitude of a bead at a single driving frequency: (a) shows the amplitude (in units of g) as a function of time, (b) is the power spectra for this time trace. The bead is a distance of 4 cm from the driving plate. The dotted line has slope of -2. (Data reproduced with permission of the authors of Ref. [10]).

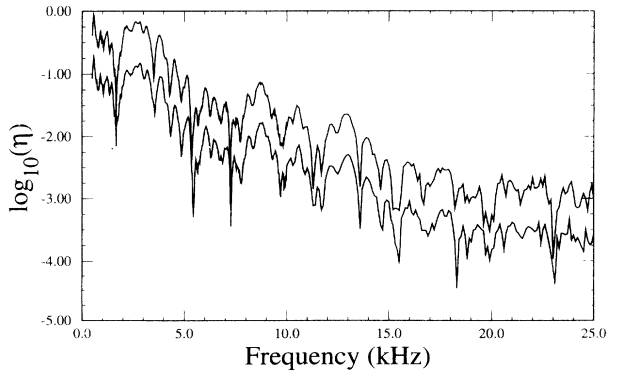

FIG. 2. Experimental results for the frequency response of a bead as a function of driving frequency. The bead is again a distance of 4 cm from the driving plate. The two curves result from successive measurements on an undisturbed system. The second curve is displaced downward so that the two are distinguishable. (Data reproduced with permission of the authors of Ref. [10].)

shown were done in consecutive sweeps through the frequency range where the measurements are separated by a short interval of time. The second curve is displaced vertically downward so that the two curves can be distinguished. If the sample was disturbed between the measurements, the response curve looked very different for the second scan of the frequency range. Thus, while the data looks "noisy," the response is actually characteristic of the particular contact network of the sample. Thus, Fig. 2 gives information about a static force network in the bead pack. Figure 1, on the other hand, results from the time evolution of this network.

In the rest of this work, I present the details of a ball and spring model for the bead pack and present numerical results for a direct comparison between the model system and the experimental results. I also study the role that the system's normal modes play in the frequency response. The rest of the paper will be organized as follows. Section II contains a discussion and motivation for this model of a granular system. In Sec. III, I will consider the continuum limit of this model and examine the solution to the differential equations which describe a homogeneous system. Section IV presents the numerical solution of the discrete model, and compares these results with the frequency response seen in the experiment. In Sec. V, I present a toy model for the slow amplitude modulations which are a result of the relaxation of the force network. Finally, in Sec. VI, I summarize and discuss extensions to this simple model which must be made to capture more of the physical characteristics of the real system.

II. BALL AND SPRING MODEL

Consider the bead pack at equilibrium. In this experiment, the only important forces acting on each bead are the contact forces between adjacent particles and gravity. The collection of contact forces among neighboring beads will be referred to as the contact force network, and the force between two connected beads will sometimes be called a "bond."

The fundamental unit of this network is the bond between two spheres. If two spherical beads are compressed together with a contact force F_c, then under the action of this force the distance between the centers of the two spheres is decreased by an amount h. For the case of linear elasticity and perfectly smooth spheres, these two quantities are related by

$$F_c = kh^{3/2} , \tag{2.1}$$

where k is a proportionality constant depending on the radii of the two spheres and their material properties [11]. For the case of an almost monodisperse collection of beads, this constant k can be treated as the same for all contacts.

Consider now an additional force δF acting on these two balls. The spheres will move together by an additional amount δh. Under this new force, Eq. (2.1) becomes

$$F_c + \delta F = k(h + \delta h)^{3/2} . \tag{2.2}$$

For the case of small δh, I can expand the expression in

parenthesis and, making use of Eq. (2.1), I find

$$\delta F = \frac{3kh^{1/2}}{2}\delta h \equiv K_h \delta h \ , \tag{2.3}$$

where K_h is a constant which depends on the equilibrium stress on each bond in the network. Equation (2.3) shows that for a sufficiently small displacement δh the bond between a pair of connected beads acts like a simple spring.

Unfortunately, (2.3) is not true for all bonds. There may exist some beads which in equilibrium are very close to each other, but are not in contact. However, under the action of δF these beads do come into contact. The experimental results indicate that this is not an important effect in understanding the response of the system. These contacts produce a force that only acts during part of the oscillation cycle. If this effect were important, then the response of the accelerometer would not be sinusoidal, but would take on some more complicated wave form. Thus, in order to understand the experimental results described above, I will not consider these "sometimes" bonds.

Finally, one might object to the use of Eq. (2.1) on the basis that it ignores the effect of the surface roughness of the beads. However, the essential idea is that for small oscillations the contact will behave like a spring, and this does not depend on the fact that the contact is Hertzian. In order to do the expansion for small δh, all that is needed is analytic behavior near equilibrium. The dependence then of K_h on the equilibrium configuration may be very complicated; however, I will not need the exact form for K_h in this study.

In terms of the response to small oscillations, the system can then be viewed as a collection of balls connected by springs, with the spring constants determined in some way by the force network of the equilibrium system. When the amplitude of a ball changes as a function of time, this indicates that the equilibrium configuration of the system has changed—the network has relaxed. The experimental results then raise some very interesting questions: What information about the force network is reflected in Figs. 1 and 2? How does the network relax in time? What is the role of the geometrical disorder in the system? These are the questions that I address in this study.

I focus on an extremely simple model for the system. For computational ease, I consider a network embedded in two spatial dimensions. I ignore the positional disorder of the grains, and consider the network topology to be that of a square lattice. I choose a velocity-dependent dissipation with a uniform damping constant. The only disorder present in the system is in the distribution of spring constants, K_h. This paper will compare the response of this model system to the response observed in the experiments.

I now present the mathematical formulation of this ball and spring model. Consider the beads, confined to a two-dimensional square lattice as in Fig. 3. I let the driving force be a sinusoidal motion of one entire wall. The sheering of two grains in contact with each other will produce dissipation in the system. I choose to include this behavior in the simplest possible way by assuming an

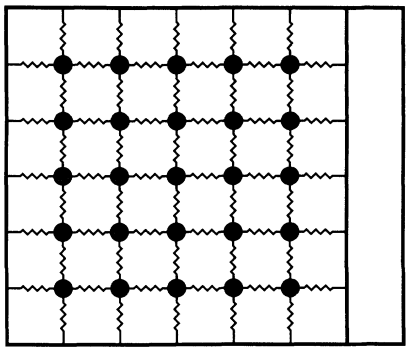

FIG. 3. Basic ball and spring model for the system. The wall on the right oscillates to provide the driving force.

interparticle damping force that is linearly dependent on the velocity difference between two adjacent beads. The final simplification comes from an assumption that the motion is decoupled in the x and y directions. This will be true in the limit of very small oscillations.

In this model, the displacement $u(p)$ of a bead at position $p=(x,y)$ is given by the differential equation

$$m\frac{d^2u(p)}{dt^2} = \sum_{p'} K_h(p,p')[u(p')-u(p)] + \sum_{p'} \beta\left[\frac{du(p')}{dt} - \frac{du(p)}{dt}\right] , \tag{2.4}$$

where m is the mass of a ball, p' is a nearest neighbors to point p, β is the damping constant, and $K_h(p,p') = K_h(p',p)$ is the spring constant between p and p'.

For boundary conditions, I take that $u(p)=0$ on all walls that do not supply a driving force. For the oscillating wall, I have the form $u(p)=\exp(i\omega t)$, where, without loss of generality, I have taken the amplitude of the wall's vibration to be unity.

It is possible to take Eq. (2.4) as the starting point for numerical investigation by merely integrating this equation to find out the response of each ball as a function of frequency. However, this does not take advantage of the fact that for small amplitude vibrations, the harmonic driving force produces harmonic motion of the particles in the bead pack. Thus, I know that the solution of interest takes the form $u(p)=A(p)\exp(i\omega t)$, where $A(p)$ is the complex amplitude for the vibration at point p. Combining this with Eq. (2.4), I find

$$m\omega^2 A(p) + \sum_{p'} [K_h(p,p') + i\omega\beta][A(p') - A(p)] = 0 \ . \tag{2.5}$$

The boundary conditions for this equation are that $A(p)=0$ on the three fixed boundaries, and that $A(p)=1$ on the oscillating wall. This equation described the steady-state response of this ball and spring model. To find the frequency response for a given system, it is necessary to know the values of $K_h(p,p')$.

III. THE CONTINUUM SYSTEM

If I consider the case of infinitesimally small particles (i.e., the continuum limit), it is possible to rewrite Eq. (2.5) in terms of a differential equation. The resulting equation can be solved exactly for the case of a uniform spring constant. Letting $K_h(p,p')=K_0$ for all p and p', I write $A(p)$ as $A(x,y)$ and consider a box with x and y dimensions L_x and width L_y, respectively. For such a system, (2.5) becomes

$$\rho\omega^2 A(x,y)+(K_0+i\omega\beta)\nabla^2 A(x,y)=0 , \tag{3.1}$$

where ρ is the mass density. The boundary conditions for this equation are $A(L_x,y)=1$ and $A(x,0)=A(x,L_y)=A(0,y)=0$. The solution to this equation, with these boundary conditions, can be obtained by standard separation of variable techniques, and I find

$$A(x,y)=\frac{4}{\pi}\sum_{n=0}^{\infty}\frac{\sin[(2n+1)\pi y/L_y]}{(2n+1)}\left[\frac{\sinh(\alpha_n x/L_x)}{\sinh(\alpha_n)}\right] , \tag{3.2}$$

where α_n is defined by

$$\alpha_n^2/L_x^2=(2n+1)^2\pi^2/L_y^2-\frac{\rho\omega^2}{K_0+i\omega\beta} . \tag{3.3}$$

It is very simple to sum this series numerically, and find the amplitude as a function of frequency for any point in the box. All that is necessary is to choose values for the parameters ρ, K_0, β, L_x, and L_y. In the solutions shown here, I choose $\rho=1$, $K_0=1$, $L_x=L_y=1$ (this defines a system of units in which ω is dimensionless). Figure 4 shows the frequency response at $(x,y)=(0.47,0.53)$ for two different values of β. In Fig. 4(a), I show the results for $\beta=0$. There is a set of frequencies where the amplitude at (x,y) is peaked, and is much greater than the amplitude of the driving wall. Additionally, there are frequencies at which the amplitude jumps discontinuously. The frequencies ω_p at which these peaks and discontinuities occur are well described by the expression

$$\omega_p^2=\pi^2[n_1^2+(2n_2+1)^2] , \tag{3.4}$$

where $n_1>0$ and $n_2>0$ are both integers. The frequencies defined by (3.4) are shown in Fig. 4(a) by the pluses located on the x axis.

The importance of these frequencies can be understood in two ways. The first comes from a direct examination of (3.2) and (3.3). At $\omega=\omega_p$ (and $\beta=0$), the value of $\alpha_{n_2}=n_1\pi i$. For this value of α_n, the function $\sinh(\alpha_n)$ vanishes, and the contribution from the $n=n_2$ term in the series (3.2) goes to infinity.

However, the frequencies of (3.4) also correspond to natural frequencies of the unforced system. Let $\beta=0$ and $A(L_x,y)=0$. In this case, Eq. (3.1) becomes an eigenvalue problem, and the eigenfunctions, $f_i(x,y)$ are

$$f_i(x,y)=\sin(q_1\pi x/L_x)\sin(q_2\pi y/L_y) , \tag{3.5}$$

with the corresponding eigenvalues ω_i^2 given by

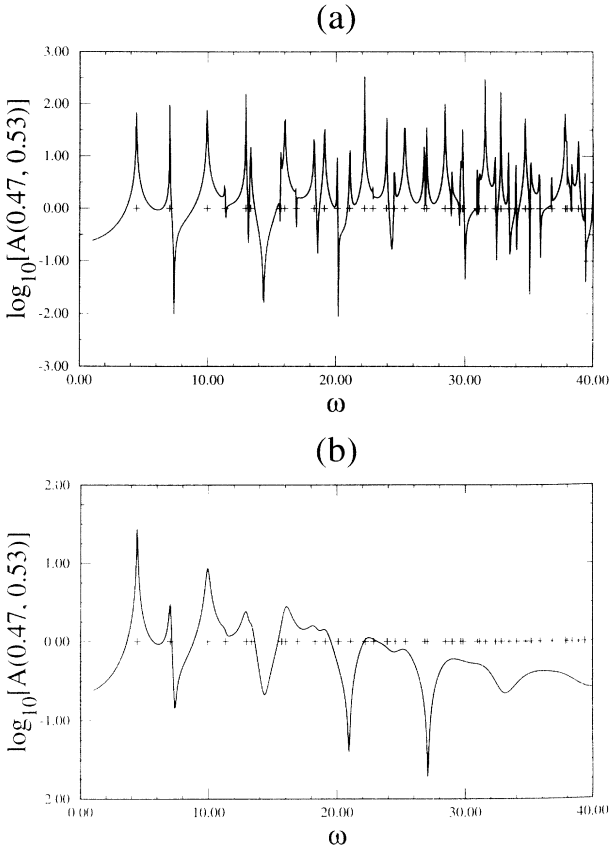

FIG. 4. Frequency response of the homogeneous system: (a) shows the response of the system with a damping coefficient $\beta=0$; (b) shows the response with damping coefficient $\beta=0.003$.

$$\omega_i^2=\frac{K_0\pi^2}{\rho}\left[\frac{q_1^2}{L_x^2}+\frac{q_2^2}{L_y^2}\right] , \tag{3.6}$$

where again $q_1>0$ and $q_2>0$ are both integers. Not all eigenfrequencies given by Eq. (3.6) are manifested in the system. This is due to the symmetry of the driving force—it is symmetric about a horizontal axis at the center of the box. This excludes all of the eigenmodes which are asymmetric about this axis (i.e., have an even value for q_2).

Figure 4(b) shows the response for a finite value of the damping coefficient, $\beta=0.003$. The frequencies defined by (3.4) are again shown as pluses along the x axis. There are two differences between this response curve and Fig. 4(a). The first is that there is an overall decrease in response as the frequency increases. This reflects the fact that the damping force is proportional to ω, and thus the damping force gets larger at higher frequencies. By looking at a larger range in frequency, it is clear that this trend is nothing as straightforward as a simple exponential decay.

The second interesting feature is the set of peaks and valleys which are superimposed on this decreasing response curve. The lowest-frequency excitations are still identifiable as distinct entities with peaks clearly occurring at the resonance frequencies. The higher-frequency

modes, on the other hand, cannot be distinguished in the response curve. The finite value of the damping term causes the resonance peaks to be greatly decreased in magnitude, and to be much broader in terms of their frequency response. At higher frequencies, many broad peaks are superposed to get the measured response of the system. It is the inhomogeneities in the distribution of these resonances that cause the apparent small peaks and valleys at high frequencies. At even higher frequencies, the effects of the damping become dominant, and the curve becomes smooth.

This is indeed reminiscent of the frequency response in the experimental system. There is a general trend of a decreasing amplitude with increasing frequency, with peaks and valleys superimposed on this decreasing curve. In the experiments, these oscillations are much more striking than in this uniform system, but the character of the response is the same.

IV. THE DISCRETE MODEL

I now study Eq. (2.5) numerically, looking at the properties of the solution for a particular distribution for the values of $K_h(p,p')$. Such a computational study involves a discrete rather than a continuum system. For the case of a square lattice, the amplitude $A(p)$ becomes $A(i,j)$, where i indicates the x coordinate of a ball, and j the y coordinate. Equation (2.5) then becomes

$$m\omega^2 A(i,j)+\sum_{(i',j')}[K_h(i,j,i',j')+i\omega\beta] \times[A(i',j')-A(i,j)]=0 , \quad (4.1)$$

where (i',j') are nearest neighbors to the ball at (i,j), and $K_h(i,j,i',j')$ is the spring constant for the bond connecting these two balls. The boundary conditions for the system are

$$A(N+1,j)=1 ,$$
$$A(0,j)=A(i,0)=A(i,N+1)=0 . \quad (4.2)$$

The first equation represents the driving wall, while the final three are for the fixed walls.

The method that I use to find the solutions of Eq. (4.1) is the biconjugate gradient method [12]. This method determines solutions to a matrix equation of the form

$$Mx=b , \quad (4.3)$$

by finding the minimum of the function $g(x)=\frac{1}{2}\bar{x}Mx-bx$. In order to transform Eq. (4.1) into the form of (4.3), it is necessary to write (4.1) as an equation for its real and imaginary parts. As a result, the matrix M is not symmetric, and this is why the biconjugate, rather than the conjugate, gradient method must be used. In my simulations, the amplitude for each point is accurate to 1 part in 10 000.

It is, of course, possible to simply invert the matrix M to find the solution. Unfortunately, the amplitude $A(i,j)$ depends on the value of the frequency, and thus, for each value of ω a completely new matrix inversion must take place. Because the amplitude has a real and imaginary part, the matrix M which describes a 20×20 system of balls is an 800×800 array. The biconjugate gradient method, on the other hand, takes advantage of the sparseness of this discretized-Laplacian type matrix, and the solution can be achieved to the desired accuracy in a much shorter period of time. All of the calculations for the results shown in this paper were done using a Sun SPARCstation IPX using approximately 150 h of CPU time.

All that remains is to choose a distribution for the set of $\{K_h(p,p')\}$. For simplicity, I take a random distribution of values on the interval $[0,K_{\max}]$. The results that I show are for a square array of balls of size 20×20. Figure 5 shows the spring configuration for the array that has been used for the results presented below. Black indicates that $K_h=K_{\max}$, while white means $K_h=0$, with a linear gray scale for intermediate values.

I choose $K_{\max}=0.25$, $\beta=0.002$ and measure the response in the frequency range $\omega=(0.01,1.3)$. I shall show below how to assign physical units to these quantities. Figure 6 shows the amplitude for a ball near the center of the pack of the springs (the precise position of the ball is indicated in Fig. 5).

There are three distinct regimes of behavior. At very low frequencies [Fig. 6(a)], the behavior is very similar to the response seen at low frequencies in the continuum case. There are frequencies at which peaks occur, and these peaks show little overlap.

In the intermediate frequency range [Fig. 6(b)], the response of the system is qualitatively the same as that shown in the experimental results of Fig. 2. There is an overall decrease of the response, and an irregular set of peaks and valleys.

For $\omega>1$ [Fig. 6(c)], the response becomes very smooth and decreases very quickly. The change in response at $\omega\approx1$ can be understood intuitively. Consider a single ball attached to four springs all with $K_h=K_{\max}$. Such a

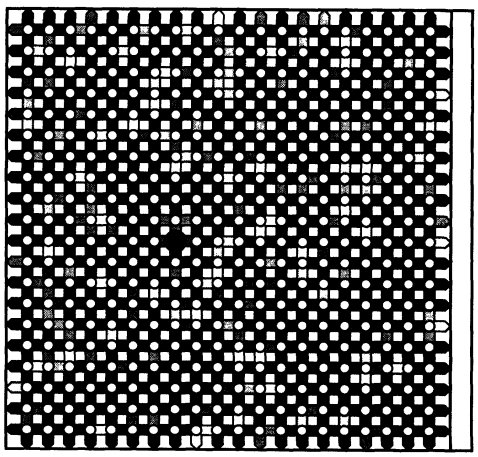

FIG. 5. The 20×20 ball and spring system used for these simulations. The intensity indicates the strength of the bond connecting two balls: black indicates that $K_h=K_{\max}$, white indicates $K_h=0$, with a linear gray scale for intermediate values. The large black ball at (8,10) indicates the location where all of the measurements occur.

ball will have its fundamental excitation at a frequency

$$\omega_{\max}=\sqrt{4K_{\max}/m} \ . \tag{4.4}$$

This then is the "natural" frequency (known as the Einstein frequency [13]) for a ball which, by chance, happens to be surrounded by springs all of which have $K_h \approx K_{\max}$. Equation (4.4) then defines the highest frequency at which any bead will naturally oscillate. Any higher-frequency oscillations would require every neighbor to vibrate in opposition with many of its neighboring particles. Below it is shown that this results in a distinctly different character to the system's oscillations.

For the values of $K_{\max}$ and m given above, $\omega_{\max}=1.0$. For other simulations, with different values for $K_{\max}$, I found that this drastic change in the response of the system occurred at the frequency given by Eq. (4.4). This frequency determines the frequency scale for the system, and I will consider my frequency as measured in units of $\omega_{\max}$. Experimentally, $\omega_{\max}$ might be measured by finding the frequency at which this rapid decrease in the response occurs. It is also possible to estimate a lower limit for $\omega_{\max}$ in the experimental system by assuming the Hertzian contact law and that contact force between any two beads is not significantly greater than the weight of a single bead. Making use of some of the information about the beads given in Ref. [10], and Eqs. (2.1), (2.3), and (4.4), I find that

$$\omega_{\max} > 45\,000 \ \text{sec}^{-1} \ , \tag{4.5}$$

which is above the observed range in the experiment.

Consider now the phase of a given ball in the array. Figure 7 is a plot of the phase versus frequency for the same ball as was used in Fig. 6. Again there is distinctly different behavior for $\omega > \omega_{\max}$. There is also a linear regime in the phase for $0.3\omega_{\max} < \omega < \omega_{\max}$. A linear relationship between the observed phase and the driving frequency is seen experimentally [14]. A simple calculation shows that for a constant group velocity v_g, the relationship between the frequency of the oscillation and the observed phase at a point should be linear. If the magnitude of the slope in the phase response curve is μ, then the group velocity is given by

$$v_g = X/\mu \ , \tag{4.6}$$

where X is the distance from the source of the driving to the point of observation. In the data shown here, the value of X is 12 particle diameters. In the experimental system, the particle diameter is 0.5 cm. Using this value and the slope from Fig. 7, I find that

$$v_g \approx 0.03\omega_{\max} \ , \tag{4.7}$$

where $\omega_{\max}$ is measured in sec^{-1}, and the group velocity

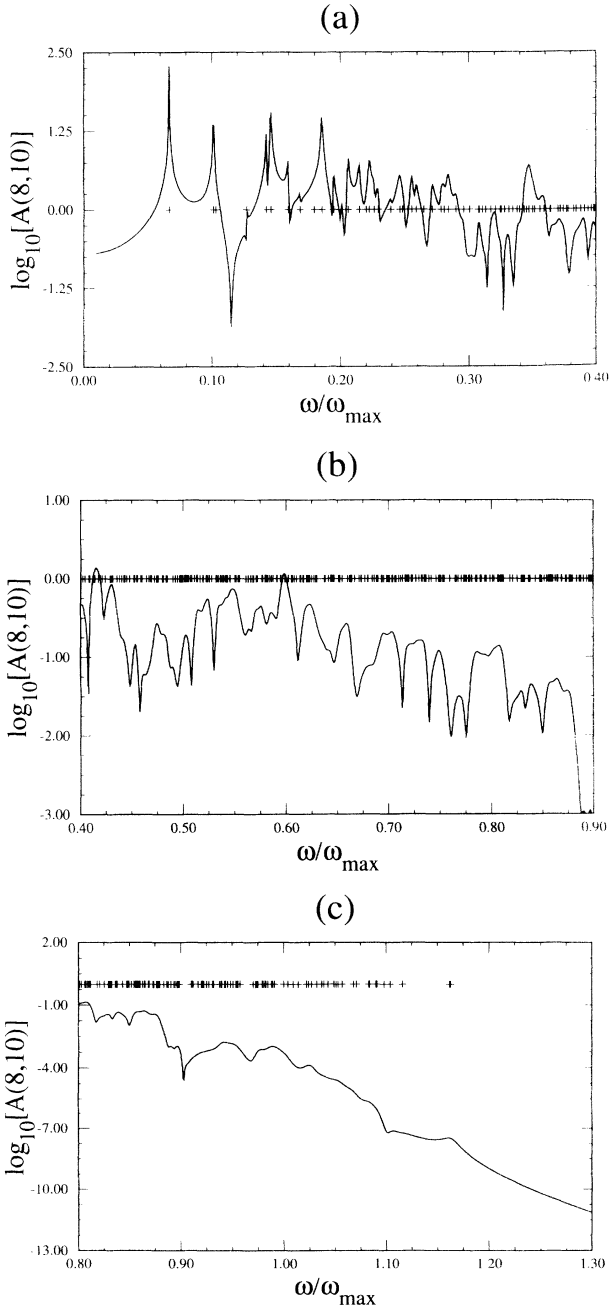

FIG. 6. Frequency response of ball at (8,10) as a function of frequency: (a) for low frequencies; (b) for intermediate frequencies; and (c) for high frequencies. The pluses along the x axis indicate the frequencies of the normal modes.

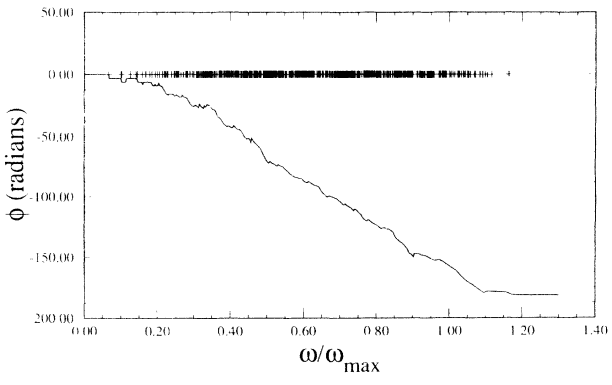

FIG. 7. Phase of a single ball for all driving frequencies. There is a linear regime in the intermediate frequency range. The pluses along the x axis mark the frequencies of the normal modes.

is given in units of cm/sec. In the experimental system, $v_g = 57$ m/sec. Matching to that velocity implies that

$$\omega_{\max} \approx 200\,000 \text{ sec}^{-1} , \tag{4.8}$$

which is clearly beyond the experimental regime. With this value of $\omega_{\max}$, Fig. 6 indicates that the typical change in frequency between the very large drops in the response is $\Delta\omega \approx 10\,000$ sec^{-1}. This compares with the experimental value which is quoted as $\Delta\omega \approx 3000$ sec^{-1}.

The parameters m and $K_{\max}$ determine the value of $\omega_{\max}$ through (4.4). The only parameter whose effect I have not discussed is the damping constant β. The value observed for μ depends sensitively on the value chosen for β. If a smaller value for β is chosen, the value of μ is increased. Additionally, a smaller β results in many more small peaks in the frequency response data, but the sharp decreases are much shallower. If, on the other hand, the value of β is increased, the sharp decreases in the response are much deeper, but they occur with a much larger spacing in frequency. The effects on the peaks can be understood by considering the results from the normal mode analysis below.

Because the normal modes proved to be so important in the response of the continuum system, I consider their manifestation in the discrete case. I again use the spring configuration of Fig. 5. Because there are 20×20 balls that are free to move this will produce 400 eigenmodes for the system. The normal modes are calculated for the undamped system with the zero amplitude boundary conditions at all walls. These calculations were done using the appropriate subroutines from EISPACK.

The easiest way to see that it is the normal modes of the zero amplitude boundary condition that determine the system behavior is to consider the much simpler system of a string driven at one end by a sinusoidal vertical displacement $\sin(\omega t)$. Assuming that the horizontal vibrations can be written as $y(x)\sin(\omega t)$, then the differential equation for $y(x)$ is

$$\frac{d^2y(x)}{dx^2} + \kappa^2 y = 0 , \tag{4.9}$$

where κ is related to the elastic properties of the string and the driving frequency. If the driving occurs at $x = L$, then boundary conditions are $y(L) = 1$ and $y(0) = 0$. The solution to this equation is $y(x) = Y \sin(\kappa x)$ where $Y = 1/\sin(\kappa L)$. The value of Y becomes very large as the value of κ approaches $n\pi/L$, where n is the positive integer. These are exactly the eigenvalues of the zero amplitude boundary-value problem. At these frequencies, the solutions also take on the form of the corresponding normal modes.

Figure 8 shows three eigenmodes for the system. The first one is the second lowest-frequency mode of the system, and shows little trace of the local nonuniformities of the network. The second mode is in the middle of the spectrum at $\omega = 0.6053\omega_{\max}$. The picture shows that the oscillation is partially, but not completely, localized. The final mode shown has $\omega = 1.000\omega_{\max}$, and there is striking localization of this mode. This is true of all the modes at high frequency, and this is the reason for the significant change in the response function at driving frequencies with $\omega > \omega_{\max}$.

These normal mode frequencies are shown as pluses in Figs. 6 and 7. Notice, as in the continuum case, that at low frequencies the sparseness of the normal mode allows them to be observed as distinct excitations of the system. At higher frequencies, however, the modes overlap and there can be no one-to-one identification between the structures in the response and a given normal mode.

Note also that the density of modes becomes very low for frequencies greater than $\omega \approx \omega_{\max}$. From the results for low frequencies, this would seem to suggest that these modes should be seen distinctly in the response curve. However, because these modes are highly localized, they will only be seen in the response if the detector happens to be inside the region of space where the mode has a nonzero value.

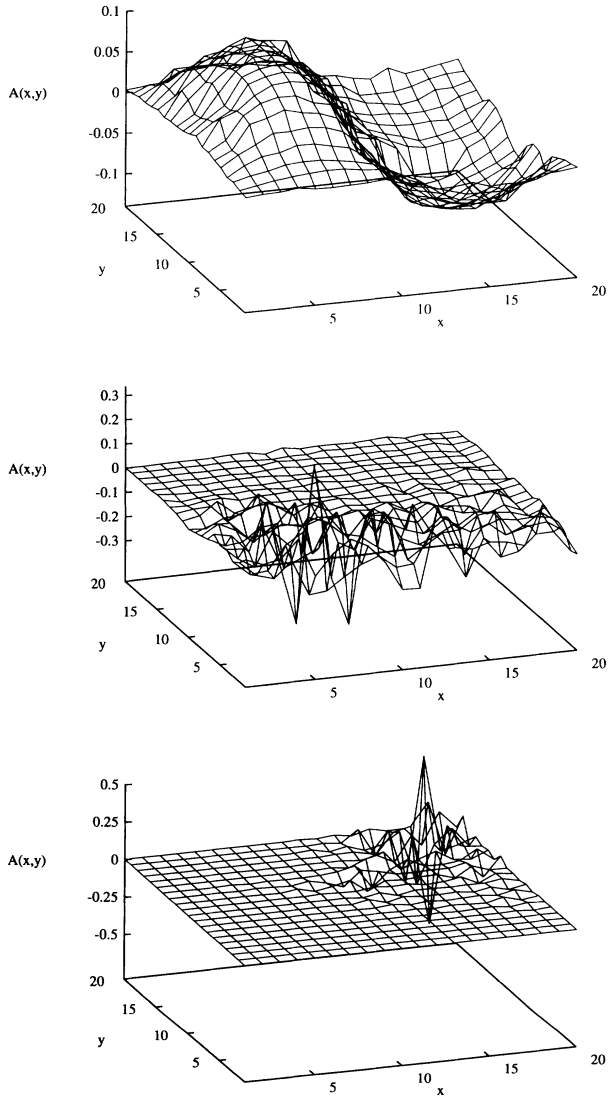

FIG. 8. Typical modes for the system in three frequency ranges: (a) $\omega = 0.1013\omega_{\max}$; the mode is extended; (b) $\omega = 0.6053\omega_{\max}$; the mode shows some localization; (c) $\omega = 1.000\omega_{\max}$; the mode is very localized.

The major difference in this nonuniform system is that not all modes will contribute equally to the system's response. A high-frequency mode which has its amplitude localized far from the driving wall is much less important than a mode which is localized near the driving wall. Thus, not only are the functional forms of the normal modes more complicated, it is also important to know which modes make the dominant contributions at each frequency.

In order to measure the contribution of each mode to the system response, I use the set of normal modes as a set of basis vectors to describe the amplitudes of the balls at each driving frequency. At a given driving frequency ω, the amplitude of the oscillations can be written as a superposition of the eigenmodes,

$$A(i,j)=\sum_{k=1}^{N\times N} c_k f_k(i,j) , \tag{4.10}$$

where in this case both i and j can only take on values between 1 and N. The coefficients c_k are given by

$$c_k=\sum_{i=1}^{N}\sum_{j=1}^{N} A(i,j) f_k(i,j) . \tag{4.11}$$

Note that the sums over i and j do not include the boundaries but only the sites interior to the system. The c_k's then give the contributions of each normal mode to the oscillations inside the system.

With the modes calculated numerically, it is a simple matter to calculate the values of c_k for each driving frequency. Figure 9 shows the values of the $|c_k|$ versus ω_k at a driving frequency $\omega=0.6\omega_{\max}$. While it is clear that the most important contributions come from the modes that have $\omega_k\approx\omega$, the structure of the curve is complicated. It is also clear that the level of a modes excitation is not simply determined by the value of $|\omega-\omega_k|$.

There are, however, some general patterns to these c_k's. Figure 10 shows the frequency of the mode that has the largest value of $|c_k|$ at each driving frequency. This is a linear function with slope 1, and indicates that the most important mode is one which has its resonant frequency near the driving frequency. Again, it is clear that the behavior sharply changes at $\omega\approx\omega_{\max}$.

Finally, I consider the c_k's for several eigenmodes

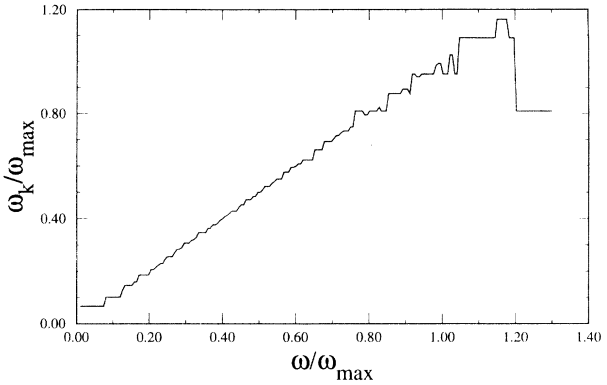

FIG. 10. The most important modes. This figure shows the value of ω_k versus the driving frequency ω for the mode which has the largest value of $|c_k|$ at each value of the value for ω. Note that above $\omega=\omega_{\max}$, the linear behavior starts to break down and the curve becomes very irregular.

which have their frequencies very close together. Shown in Fig. 11 are the values of the $|c_k|$ as a function of frequency for three modes with a resonance frequency near $\omega=0.6\omega_{\max}$. Each curve shows a clear resonance behavior when the driving frequency approaches its natural frequency. However, it is clear that each mode is excited to a different degree by the driving force.

As was stated above, it is possible to understand the changes in the response curve as the value β is changed by considering the normal mode. When the value of β is decreased, each of these modes will have a much sharper peak in its c_k when the driving frequency approaches the mode's natural frequency. Thus, any mode which has a nonzero contribution to the amplitude at the detector is more likely to make its presence felt. Thus, there are many more smaller peaks in the measured response.

V. TOY MODEL FOR RELAXATION

Because (2.5) is a steady-state solution for fixed ω, there will be only one amplitude measured for all time. I have allowed for no relaxation of the lattice which is the source of the behavior in Fig. 1. As a toy model for this relaxation process, I consider the amplitude at one point,

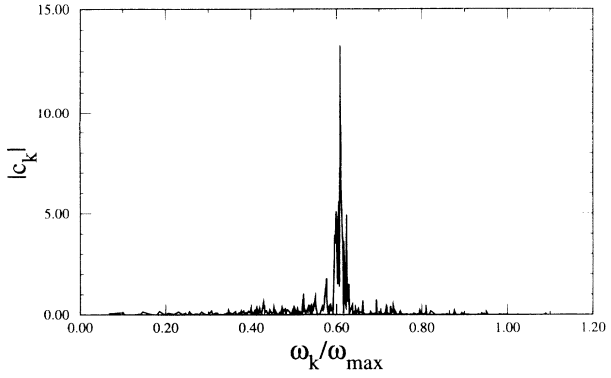

FIG. 9. Values for the $|c_k|$'s as a function of the mode frequency ω_k. The driving frequency is $\omega=0.6\omega_{\max}$.

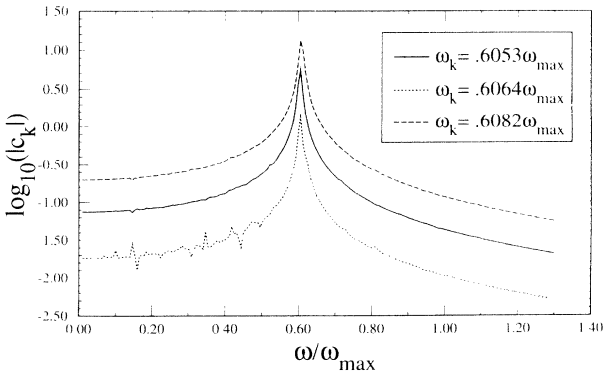

FIG. 11. The value of $|c_k|$ as a function of the driving frequency ω for three successive modes of the system.

while randomly changing one bond per unit of time τ. This bond is assigned a new random value between 0 and K_{max}. Having changed one of the values of K_h, I then find the new solution of (2.5). This new solution has a different value for the observed amplitude, and by plotting this as a function of elapsed time, I generate a time sequence. I then compare the power spectra of this series to the experimental power spectra.

I begin the simulations with the same bond configuration as shown in Fig. 5, and measure the amplitude of the same ball as I used for the frequency data. The system is driven with an oscillation of frequency $\omega=0.6\omega_{max}$, with a value of $\beta=0.01$. The amplitude of the vibration as a function of time is shown in Fig. 12(a). Using a much longer time series, I can calculate the power spectrum, $S(f)$, for this time series [15], with the results shown in Fig. 12(b). There is a clear power-law behavior in the power spectrum. If the power spectrum is written as $S(f)\sim f^{-\psi}$, I then find that $\psi\approx 1.9$ over a region of one and a half decades. This is fair agreement with the experiments, which find values for ψ between 2 and 2.2.

It is not surprising that $\psi\approx 2$ in both the toy model and the real system for the following reason [10]. Imagine that at one time the amplitude of the detector has some value B_0 and then one of the bonds is changed. This will either raise or lower the observed amplitude by ΔB_0, and I might expect, in general, that the change might be equally likely to cause an increase as a decrease. Then another bond is changed, and the amplitude changes by some amount $\pm\Delta B_1$. In this picture it is clear that the amplitude is executing a random walk. Such a time trace is known to have a power spectrum with an exponent $\psi=2$. Thus, the power-law behavior is not surprising, and the exponent near 2 seems to be intuitive.

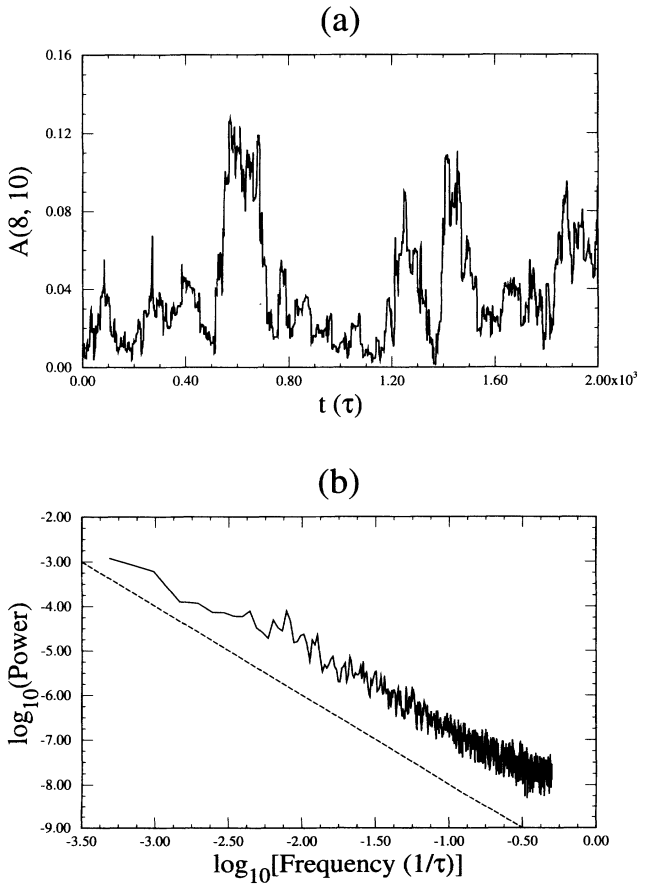

FIG. 12. Results for the time trace of the amplitude as the bond network is changed: (a) is a sample of the time trace data; (b) shows the corresponding power spectra. A line with slope -2 is shown for comparison.

There are, however, several assumptions in this argument which are unjustified. Are B and ΔB actually uncorrelated? Are successive values for ΔB uncorrelated? In order to understand the experimentally observed results, a more physically motivated process for the network relaxation is necessary.

VI. CONCLUSIONS AND DISCUSSION

The principal objective of this paper is to show that the vibrational properties of a granular material can be reproduced with a simple linear ball and spring model. I have been able to reproduce qualitatively the frequency response of a single grain to a sinusoidal driving frequency. There is as yet no way to make a quantitative comparison with experiments, because there is no well-defined method for characterizing the statistical properties of the "noisy" response curve. The normal-mode analysis indicates that the peaks in the spectrum cannot be associated on a one-to-one basis with a resonance of the system; however, it is clear that the behavior at a given frequency is a result of a superposition of the normal modes which have their resonance frequencies in the regime of the driving frequency. The toy model for the relaxation of the lattice does reproduce a power law in the behavior in the power spectrum. The fact that the model is simple, and yet produces the experimentally observed behavior, suggests that it may be worth studying in its own right.

One obvious simplification of this model is its two-dimensional character. It is not clear how things will change in three dimensions. The properties of localization are known to depend on dimensionality [3]. The computational difficulty with examining the three-dimensional case simply comes from the size of the matrices involved (e.g., a $10\times10\times10$ set of balls would require the inversion of a 2000×2000 element matrix for each value of ω).

However, there is another more fundamental aspect of the real system that cannot be studied with this simple ball and spring model—the experiments show an extreme sensitivity to thermal fluctuations. In additional measurements, Liu and Nagel place within the sample a small heater the size of a single bead, and they run a heat pulse through it [14]. The pulse changes the temperature of single bead by approximately 0.8 K, and they find that the response of the distant accelerometer changes almost instantaneously by 25%. The effect of the change in temperature is to change, by thermal expansion, the size of the beads in a region near the heater. The change in radius of the bead is estimated at 1000 Å. In order to understand these temperature effects, a much more physi-

cally motivated model is needed for the granular system.

Another defect with the current model is that it does not allow for a general topology for the force network. Also, the spring constants are clearly determined by the different equilibrium forces on the beads. However, there is no requirement that these forces sum to zero, as they should in equilibrium. This problem can only be solved by choosing a specific form for the force law between touching spheres. Once these problems are solved, it would be straightforward to study the effects of local thermal fluctuations.

ACKNOWLEDGMENTS

I would like to gratefully acknowledge Thomas Witten and Jysoo Lee for invaluable conversations and suggestions. I would also like to thank Chu-heng Liu and Sid Nagel for providing me with the latest results from their experiments, and for many useful discussions. I also thank H. Nakanishi, T. C. Halsey, M. Marder, H. Herrmann, M. Gannon, A. Kolan, C. Moukarzel, K. Lauritsen, and S. Melin.

[1] H. Jaeger and S. Nagel, Science **255**, 1523 (1992).
[2] P. Anderson, Phys. Rev. **109**, 1492 (1958).
[3] B. Souillard, in *Chance and Matter, Les Houches 1986, Session XLVI,* edited by J. Souletie, J. Vannimenus, and R. Stora (North-Holland, Amsterdam, 1987), and references therein.
[4] P. Dean, Rev. Mod. Phys. **44**, 127 (1972), and references therein.
[5] S. Nagel, S. Rahman, and G. Grest, Phys. Rev. Lett. **47**, 1665 (1981).
[6] A. Petri and L. Pietronero Phys. Rev. B **45**, 12 864 (1992), and references therein.
[7] L. Ye, G. Cody, M. Zhou, P. Sheng, and A. Norris, Phys. Rev. Lett. **69**, 3080 (1992).
[8] J. Marion, *Classical Dynamics of Particles and Systems* (Academic, Orlando, 1977).
[9] M. Ammi, D. Bideau, and J. Troadec, J. Phys. D **20**, 424 (1987).
[10] C. Liu and S. Nagel, Phys. Rev. Lett. **86**, 2301 (1992).
[11] L. Landau and E. Lifshitz, *Theory of Elasticity* (Pergammon, London, 1959).
[12] W. Press and S. Teukolsky, Comput. Phys. **6**, 400 (1992).
[13] A. Czachor, in *Physics of Phonons: Proceedings of the XXIII Winter School of Theoretical Physics,* edited by T. Paszkiewicz (Springer-Verlag, Berlin, 1987).
[14] C. Liu and S. Nagel (unpublished).
[15] W. Press, B. Flannery, S. Teukolsky, and W. Vetterling, *Numerical Recipes: The Art of Scientific Computing* (Cambridge University Press, New York, 1988).

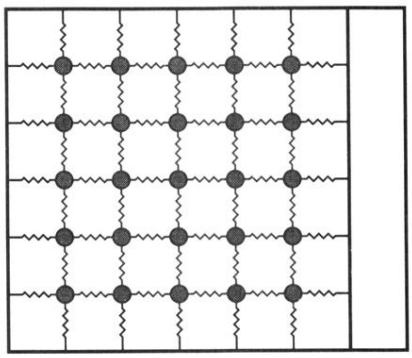

FIG. 3. Basic ball and spring model for the system. The wall on the right oscillates to provide the driving force.

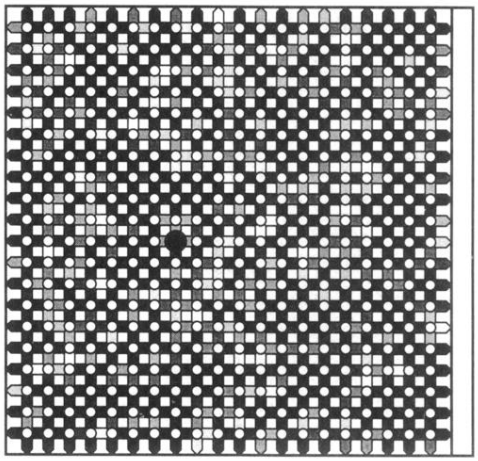

FIG. 5. The 20×20 ball and spring system used for these simulations. The intensity indicates the strength of the bond connecting two balls: black indicates that $K_h = K_{\max}$, white indicates $K_h = 0$, with a linear gray scale for intermediate values. The large black ball at (8,10) indicates the location where all of the measurements occur.